Received March 2001
Revised March 2001
Accepted August 2001

Analysis of à-posteriori error indicator in viscous flows

D.H. Wu
Sound Advantage LLC, Irvine, USA
I.G. Currie
University of Toronto, Canada

Keywords *Adaptive techniques, Acceleration, Error indicators, Navier Stokes equation*

Abstract *An à-posteriori error indicator for solving viscous incompressible flow problems is analyzed in this paper. The indicator named "velocity angle error estimator" is based on the spatial derivative of velocity direction fields and it can detect local flow features, such as vortices and separation, and resolve flow details precisely. The refinement indicator corresponds to the antisymmetric part of the deformation-rate-tensor, and it is sensitive to the second derivative of the velocity angle field. Rationality discussions reveal that the à-posteriori error indicator is a curvature error indicator, and its value reflects the accuracy of streamline curves. It is also found that the velocity angle error indicator contains the nonlinear convective term of the Navier–Stokes equations, and it identifies and computes the direction difference when the convective acceleration direction and the flow velocity direction have a disparity. Numerical simulation is presented to illustrate the use of the velocity angle error indicator.*

1. Introduction

Adaptive strategies based on à-posteriori error estimation are important in numerical simulation because they provide effective means of optimizing numerical solutions, thereby enhancing the scope of their applications (Ewing, 1990; Habashi *et al.*, 1994; Lee and Tsuei, 1992; Oden *et al.*, 1995). Most of the recent work on adaptive finite element methods using à-posteriori local projection error estimation has focused on improving the accuracy of the primary unknowns (Baker, 1997; Fuenmayor *et al.*, 1997), i.e., velocity components, temperature, etc. However, little work has been done to assess the accuracy of fluid velocity direction fields and to connect the velocity direction with flow characteristics.

The error estimation technique (Babuška *et al.*, 1994; Babuška *et al.*, 1994; Zhu, 1997) provides an assessment of accuracy of the solutions obtained by the finite element solver. In the adaptive process, meshes are automatically modified and grid cells are adjusted to match the flow and to capture the details of flow features. The generation of the velocity angle error indicator is motivated by observing the fluid flow solution, in which flow features occur as the velocity angle θ varies. By knowing the "true" θ gradient fields, a velocity angle error indicator is constructed to compute the error between the finite element approximation with the "true" derivative field. As shown in (Wu and Currie, 1997; Wu and Currie, 2000), the error indicator can efficiently resolve certain flow features, such as stagnation points, reattachment points, and

International Journal of Numerical Methods for Heat & Fluid Flow, Vol. 12 No. 3, 2002, pp. 306-327.

DOI 10.1108/09615530210422983

recirculation eddies, where velocity magnitudes are typically small. In this paper, this à-posteriori error indicator is analyzed from its mathematical properties, and discussed to reveal its linkage with viscous flow characteristics.

The plan of the paper is as follows. In Section 2 the problem is introduced and a general discussion of the à-posteriori error indicator e_θ is presented. In Section 3, the mathematical properties of the à-posteriori error indicators e_θ are described. In addition, the rationale for the velocity angle error indicator is discussed in this section. Section 4 presents numerical examples illustrating the adaptive results using the velocity angle error indicator. In Section 5, conclusions are drawn.

2. À-posteriori adaptive error indicator

The governing equations for viscous incompressible Newtonian fluids involve the conservation of mass and momentum. The primitive variable form of the Navier-Stokes equations for steady-state flow in a dimensionless form is:

$$\mathbf{u}\cdot\nabla\mathbf{u} + \nabla p - \frac{1}{Re}\nabla^2\mathbf{u} = 0 \tag{1-a}$$

$$\nabla\cdot\mathbf{u} = 0 \tag{1-b}$$

where $Re = UL/\nu$ is the Reynolds number. In the finite element formulation the velocities are approximated with quadratic shape functions and the pressure is approximated with linear shape functions on each adaptive element (Axelsson and Barker, 1984; Cuvelier *et al.*, 1986). Equation (1) is discretized from a continuous to a spatially discrete system of equations via Galerkin's technique (Girault and Raviart, 1986; Pironneau, 1989).

Based on the piecewise-continuous approximation of the velocity field, the flow direction or velocity angle is calculated as $\theta = \tan^{-1}(v/u)$ at each velocity node. The velocity angle error estimator is constructed as follows:

$$e_\theta = \sum \int_{\Omega^e} [(\hat{\theta}_x - \bar{\theta}_x)^2 + (\hat{\theta}_y - \bar{\theta}_y)^2]\, \mathrm{d}\Omega^e \tag{2}$$

where θ is the flow velocity direction computed from the velocity field, $\hat{\theta}_x = \partial\theta/\partial x$ is calculated based on the finite element derivative and has discontinuous jumps across element interfaces. $\bar{\theta}_x$ denotes a recovered smooth field (smooth $\hat{\theta}_x$ to obtain $\bar{\theta}_x$). The continuous $\bar{\theta}$ can be recovered by simply averaging the values over all the elements around each node, or by fitting the finite element solution in a least squares sense. The least squares projection (e.g. $\bar{\theta}_y$) is the following:

$$\int_\Omega \phi_i(\bar{\theta}_x - \hat{\theta}_x)\mathrm{d}\Omega = 0 \qquad \int_\Omega \phi_i(\bar{\theta}_y - \hat{\theta}_y)\mathrm{d}\Omega = 0 \quad i = 1,\ldots,N_\theta.$$

$$\bar{\theta}_x = \sum_{j=1}^{N_\theta} \phi_j \{\bar{\theta}_x\}_j \qquad \bar{\theta}_y = \sum_{j=1}^{N_\theta} \phi_j \{\bar{\theta}_y\}_j$$

$$\left(\int_\Omega \phi_i \phi_j d\Omega\right)\{\bar{\theta}_x\}_j = \int_\Omega \phi_i \hat{\theta}_x d\Omega \qquad \left(\int_\Omega \phi_i \phi_j d\Omega\right)\{\bar{\theta}_y\}_j = \int_\Omega \phi_i \hat{\theta}_y d\Omega \quad (3)$$

where $\bar{\theta}$ denotes a least squares projection; $\{\bar{\theta}_x\}_j$ and $\{\bar{\theta}_y\}_j$ denote the nodal values of the continuous θ derivative fields; $\hat{\theta}_x$ and $\hat{\theta}_y$ are the finite element approximations ($\hat{\theta}_x = \partial\theta/\partial x$ and $\hat{\theta}_y = \partial\theta/\partial y$). The details of the implementation of the velocity angle error estimator can be found in (Wu and Currie, 1997; 2000).

Both the velocity angle error estimator e_θ and the strain error estimator e_ε belong to the projection approach (Zienkiewicz and Zhu, 1987), in which e_ε, also called Zienkiewicz and Zhu error estimator, is expressed as

$$e_\varepsilon = \sum \int_{\Omega^e} [(\hat{\varepsilon}_{xx} - \bar{\varepsilon}_{xx})^2 + (\hat{\varepsilon}_{yy} - \bar{\varepsilon}_{yy})^2 + 2(\hat{\varepsilon}_{xy} - \bar{\varepsilon}_{xy})^2] d\Omega^e \quad (4)$$

where $\hat{\varepsilon}$ is the finite element derivative of velocities. Both e_θ and e_ε hold quantitative properties and are mesh independent. However, e_θ and e_ε compute different physical variables and therefore lead to different fluid flow representations. As seen from the construction of the error estimators, e_ε evolves from the u and v components which do not explicitly show the direction of a velocity vector. At the same time, e_θ evolves from the v/u ratio which directly shows fluid flow directions. On the derivative level, e_ε compares $\hat{\varepsilon}$ jumps while e_θ compares $\hat{\vartheta}$ jumps (ϑ represents the derivative of θ). e_ε is equivalent to the symmetric part of the deformation-rate-tensor and it reflects the rate of dilatation and shearing of a fluid element. e_θ is equivalent to the antisymmetric part (Ω_z) of the deformation-rate-tensor and it reflects the rate of rotation of the fluid element. It is noted that the v/u ratio is the foundation component of e_θ, and it is the ratio v/u (tangent of the velocity vector) which distinguishes the e_θ estimator from other error estimators. In the meantime, besides being a reflection of velocity directions, the v/u ratio also represents the equation of the streamlines.

As seen from Figure 1, curvature is the rate of change of direction of a curve at a particular point on that curve and is defined as $k = d\Theta/ds$. In the velocity angle error computation, θ is the velocity direction and it is defined as $\theta = \tan^{-1}(v/u)$. It is noted that $\Delta\Theta$ which is defined in the curvature of a plane curve coincides with $\Delta\theta$ in the e_θ estimator (Figure 1). Thus, θ_s is similar to ϑ since both variables are the spatial derivatives of the θ fields. A curvature error estimator which is based on comparing $\hat{\theta}_s$ and $\check{\theta}_s$, or comparing $\hat{k}$ and $\check{k}$, is seen to approach the e_θ estimator if the arc length s is small. Therefore, the properties of the mathematical quantity k can be used to interpret and understand the e_θ estimator. In the finite element computation of viscous flow,

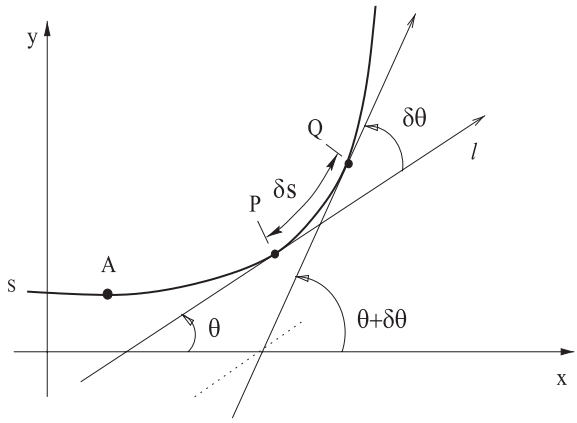

Figure 1.
The curvature of a plane curve

the velocity angle, θ, is calculated at each discretized node; and x and y are the independent variables since the Eulerian framework is used. This indicates that the curve in the e_θ computation is an instantaneous curve, and the calculated θ field represents different particles at the same time, not a particular particle at different time. Thus, in unsteady cases, the curve in the velocity angle error calculation is a streamline curve and e_θ represents the accuracy of streamlines. For steady cases, the curvature error estimator can also represent the accuracy of pathlines and streaklines.

Since the streamline is part of results in the computation of viscous incompressible flows, the connection between the velocity angle error indicator e_θ and the streamline is of use in the adaptive grid resolution of flow features. The finite element computation of a velocity field produces the approximate streamlines, or the approximate curves. Obviously, these streamline curves are not accurate due to the initial coarse grid. It is required to have the most accurate streamlines at an affordable computational cost (less unknowns). The accurate streamline curves are governed by the curvature of the curve. The velocity angle error indicator e_θ calculates the curvature error and guides the mesh density. As the adaptive levels go further, and the appropriate regions (high error regions) are identified, the velocity angle error is reduced by the denser grids in these regions. As the velocity angle error is dropped, the approximated curves or the approximated streamlines, are close to, or asymptotic to, the true curves or the true streamlines.

3. Analytical discussions

3.1 θ_x and θ_y: Convective acceleration/velocity magnitude[2]

In Cartesian coordinates, the streamlines can be expressed as $y = y(x)$. The equation of the streamline is

$$\frac{dx}{u} = \frac{dy}{v}, \quad or \quad y' = \frac{dy}{dx} = \frac{v}{u}.$$

θ is a function of x and y, and along the streamline y is a function of x, then

$$\theta = \theta(x, y) = \theta(x, y(x))$$

Differentiating θ with respect to x yields,

$$\frac{d\theta}{dx} = \frac{\partial\theta}{\partial x}\cdot\frac{dx}{dx} + \frac{\partial\theta}{\partial y}\cdot\frac{dy}{dx} = \frac{\partial\theta}{\partial x} + \frac{\partial\theta}{\partial y}\cdot\frac{v}{u} = \theta_x + \theta_y\cdot\frac{v}{u}$$

Note that θ also represents the velocity direction, and is the arctangent of the v/u ratio:

$$\theta = \theta(x, y) = \tan^{-1}\left(\frac{v}{u}\right)$$

then,

$$\frac{d\theta}{dx} = \frac{1}{1 + \left(\frac{v}{u}\right)^2}\cdot\frac{d}{dx}\left(\frac{v}{u}\right) = \frac{u^2}{u^2 + v^2}\cdot\frac{\frac{dv}{dx}\cdot u - \frac{du}{dx}\cdot v}{u^2}$$

$$= \frac{\left(\frac{\partial v}{\partial x}\frac{dx}{dx} + \frac{\partial v}{\partial y}\cdot\frac{dy}{dx}\right)\cdot u - \left(\frac{\partial u}{\partial x}\frac{dx}{dx} + \frac{\partial u}{\partial y}\cdot\frac{dy}{dx}\right)\cdot v}{u^2 + v^2}$$

$$= \frac{\left(\frac{\partial v}{\partial x} + \frac{\partial v}{\partial y}\cdot\frac{v}{u}\right)\cdot u - \left(\frac{\partial u}{\partial x} + \frac{\partial u}{\partial y}\cdot\frac{v}{u}\right)\cdot v}{u^2 + v^2}$$

Here, incompressible flow is considered ($\nabla\cdot\mathbf{u}=0$),

$$\frac{\partial u}{\partial x} + \frac{\partial v}{\partial y} = 0$$

Then,

$$\frac{d\theta}{dx} = \frac{\left(\frac{\partial v}{\partial x} - \frac{\partial u}{\partial x}\cdot\frac{v}{u}\right)\cdot u - \left(-\frac{\partial v}{\partial y} + \frac{\partial u}{\partial y}\cdot\frac{v}{u}\right)\cdot v}{u^2 + v^2} = \frac{u\frac{\partial v}{\partial x} + v\frac{\partial v}{\partial y} - \frac{v}{u}\left(u\frac{\partial u}{\partial x} + v\frac{\partial u}{\partial y}\right)}{u^2 + v^2}$$

Therefore the following relations are reached:

$$\theta_x = \frac{\partial\theta}{\partial x} = \frac{u\cdot\frac{\partial v}{\partial x} + v\cdot\frac{\partial v}{\partial y}}{u^2 + v^2} \tag{5}$$

$$\theta_y = \frac{\partial \theta}{\partial y} = \frac{u \cdot \dfrac{\partial u}{\partial x} + v \cdot \dfrac{\partial u}{\partial y}}{u^2 + v^2} \cdot (-1) \tag{6}$$

It is noted that the numerator of equation (5) is the convective term in the y-momentum, the numerator of equation (6) is the convective term in the x-momentum, and the denominator is the square of the velocity amplitude. The nonlinear convective acceleration is thus connected with θ_x and θ_y, and θ_x and θ_y constitute the velocity angle error estimator e_θ.

Denote a_x, a_y, and A as:

$$a_x = u \cdot \frac{\partial u}{\partial x} + v \cdot \frac{\partial u}{\partial y}$$

$$a_y = u \cdot \frac{\partial v}{\partial x} + v \cdot \frac{\partial v}{\partial y}$$

$$A = \sqrt{u^2 + v^2}$$

Then,

$$\theta_x = \frac{\partial \theta}{\partial x} = \frac{a_y}{A^2} \tag{7}$$

$$\theta_y = \frac{\partial \theta}{\partial y} = -\frac{a_x}{A^2} \tag{8}$$

It can be seen from Equation (7) and Equation (8) that when the velocity amplitude (A) is small and the convective acceleration (a_x or a_y) is large, θ_y or θ_x is large, and the curvature k is large too. The large variations of θ_x or θ_y generally lead to a large velocity angle error e_θ, and as a result, bring a dense grid. This situation usually happens in regions where the fluid flow is slow, but interesting flow features occur. Equation (7) and Equation (8) explain why the e_θ estimator is able to resolve these regions from a mathematical point of view.

When the velocity amplitude (A) is large and the convective acceleration (a_x or a_y) is small, θ_y or θ_x is small, and the curvature k is small too (this means that the curve is not tight). Usually in this kind of situation, variations of θ_x or θ_y are small, the e_θ error is small and no refinement is needed. This is exactly what an adaptivity criterion is expected to achieve.

When the velocity amplitude (A) is fixed, only a_x or a_y influences θ_y or θ_x. Also it can be said that the results of θ_x or θ_y affect the accuracy of a_y or a_x. Thus, the velocity angle error estimator ($e_\theta = \sum \int_{\Omega^e} [(\hat{\theta}_x - \bar{\theta}_x)^2 + (\hat{\theta}_y - \bar{\theta}_y)^2] \mathrm{d}\Omega^e$) is related to the accuracy of the convective acceleration.

Therefore, as the velocity angle error is reduced by denser grids at the appropriate regions (using the e_θ estimator), a_x and a_y become more accurate. When $\hat{\theta}_x$ is asymptotic to $\bar{\theta}_x$, or the true θ_x, the calculated value of a_y is

asymptotic to the true a_y. When $\hat{\theta}_y$ is asymptotic to $\bar{\theta}_y$, or the true θ_y, the calculated value of a_x is asymptotic to the true a_x.

3.2 Acceleration direction vs. velocity direction

The convective acceleration is a vector which has components a_x and a_y, and direction. The acceleration direction is not necessarily the same direction as the velocity direction, and the variation of θ with s yields acceleration direction as follows:

$$\theta = \theta(x,y) = \theta(x,y(x)) \quad s = s(x,y) = s(x,y(x))$$

$$\frac{\mathrm{d}\theta}{\mathrm{d}x} = \frac{\mathrm{d}\theta}{\mathrm{d}s}\cdot\frac{\mathrm{d}s}{\mathrm{d}x} = \frac{\mathrm{d}\theta}{\mathrm{d}s}\cdot\left[\frac{\partial s}{\partial x}\cdot\frac{\mathrm{d}x}{\mathrm{d}x} + \frac{\partial s}{\partial y}\cdot\frac{\mathrm{d}y}{\mathrm{d}x}\right] = \frac{\mathrm{d}\theta}{\mathrm{d}s}\cdot\left[\frac{\partial s}{\partial x} + \frac{\partial s}{\partial y}\cdot\frac{v}{u}\right]$$

where

$$\frac{\partial s}{\partial x} = \sqrt{1+(y')^2} = \frac{\sqrt{u^2+v^2}}{u} \quad \frac{\partial s}{\partial y} = \frac{\sqrt{u^2+v^2}}{v}$$

Thus,

$$\frac{\mathrm{d}\theta}{\mathrm{d}s}\cdot\left[\frac{\sqrt{u^2+v^2}}{u} + \frac{v}{u}\cdot\frac{\sqrt{u^2+v^2}}{v}\right] = \frac{\left(u\frac{\partial v}{\partial x} + v\frac{\partial v}{\partial y}\right) - \frac{v}{u}\left(u\frac{\partial u}{\partial x} + v\frac{\partial u}{\partial y}\right)}{u^2+v^2}$$

Rearrange the above equation and the following relation is reached:

$$k = \frac{\mathrm{d}\theta}{\mathrm{d}s} = \frac{\left(u\frac{\partial v}{\partial x} + v\frac{\partial v}{\partial y}\right) - \frac{v}{u}\left(u\frac{\partial u}{\partial x} + v\frac{\partial u}{\partial y}\right)}{\frac{1}{u} + \frac{v}{u}\cdot\frac{1}{v}}\cdot\frac{1}{(u^2+v^2)^{\frac{3}{2}}} \tag{9}$$

Define the symbol Λ as

$$\Lambda = (u^2+v^2)^{\frac{3}{2}}\cdot\left(\frac{1}{u} + \frac{v}{u}\cdot\frac{1}{v}\right)$$

where Λ can be roughly viewed as the square of the velocity amplitude, or $\Lambda \approx A^2$. Since $\tan\theta = v/u$, and the convective components can also be expressed as a_x and a_y, the Equation (9) can be written as:

$$k = \frac{\mathrm{d}\theta}{\mathrm{d}s} = \frac{a_y - \tan\theta\cdot a_x}{\Lambda} \tag{10}$$

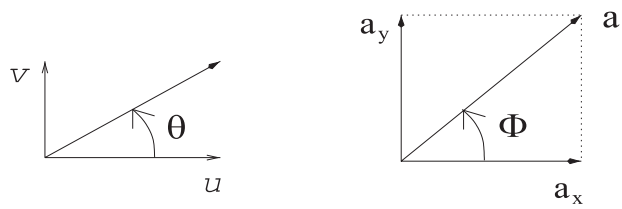

Figure 2.
Velocity direction and acceleration direction

The direction of the convective acceleration, as shown in Figure 2, is expressed as

$$\tan \Phi = \frac{a_y}{a_x} \tag{11}$$

By using $a_y = \tan \Phi \cdot a_x$, Equation (10) becomes

$$k = \frac{\mathrm{d}\theta}{\mathrm{d}s} = \frac{a_x}{\Lambda}(\tan \Phi - \tan \theta) \tag{12}$$

This indicates that the curvature k increases as a_x/Λ increases. When the acceleration direction Φ is different from the velocity direction θ, or $(\tan \Phi - \tan - \theta) \neq 0$, a curve is generated and the curvature (k) is not zero. The larger the difference between $\tan \Phi$ and $\tan \theta$, the larger is the curvature k. The larger the variation of these direction differences, the larger is the value of the velocity angle error e_θ. Obviously, when the acceleration direction is the same as the velocity direction, the curves become straight lines and $k = 0$.

By using $a_x = a_y \tan \Phi$, Equation (10) becomes

$$k = \frac{\mathrm{d}\theta}{\mathrm{d}s} = \frac{a_y}{\Lambda}\left(1 - \frac{\tan \theta}{\tan \Phi}\right) \tag{13}$$

This indicates that the curvature k increases as a_y/Λ increases. When Φ is close to θ, or $\tan \Phi$ is close to $\tan \theta$, k becomes smaller. When Φ is different from θ and $|\tan - \theta/\tan - \Phi - 1| \gg 0$, the curvature k becomes larger. When the variations of k are large, the velocity angle error e_θ becomes larger and refinement is conducted in these regions

By using $a_y = a \sin \Phi$ and $a_x = a \cos \Phi$, Equation (10) becomes

$$k = \frac{\mathrm{d}\theta}{\mathrm{d}s} = \frac{a}{\Lambda}(\tan \Phi - \tan \theta)\cos \Phi$$

This gives a relation between the velocity angle error and the convective acceleration.

As a result, when the convective acceleration direction (Φ) and the flow velocity direction (θ) become disparate, curvature k occurs ($k \neq 0$) and some kind of changes occur in the fluid flow as well. The larger the difference between $\tan \Phi$ and $\tan \theta$, the larger is the curvature k, and the larger the variation of these differences, the larger is the value of the velocity angle error. The velocity angle error estimator e_θ can identify these regions where two directions have a difference and it calculates the directional error based on this direction difference.

4. Results and discussion

4.1 Flow over a cavity

The velocity angle error indicator has been benchmarked with the analytic solution known as Kovasznay flow (Wu, 2000; Wu and Currie, 2000). This laminar flow which satisfies the steady incompressible Navier-Stokes equations with no forcing term represents the flow behind a two dimensional

grid. (Wu, 2000; Wu and Currie, 2000) also contain the validation study for the case of flow past a backward-facing step.

As an application of the adaptive refinement scheme, the flow over a cavity is first considered. The computational domain and boundary conditions are shown in Figure 3, and the width of the cavity is four times of the height of the cavity. The entrance velocity is specified by a parabolic profile and Neumann boundary conditions are imposed at the exit.

The adaptive algorithm is applied in the refinement of unstructured meshes at each adaptive level. Figure 4 shows the adaptive mesh results using the velocity angle estimator e_θ with $Re = 200$. For the same Re case, the meshes

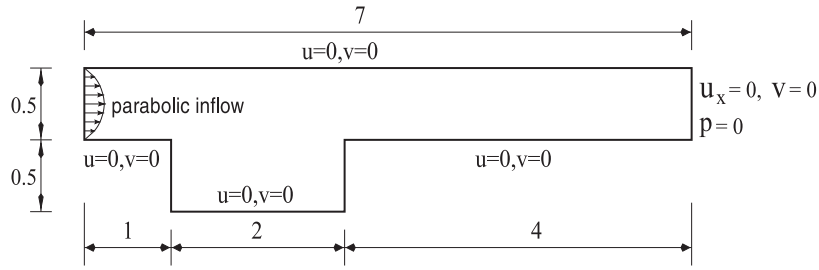

Figure 3.
Schematic of flow over a cavity (the computational domain)

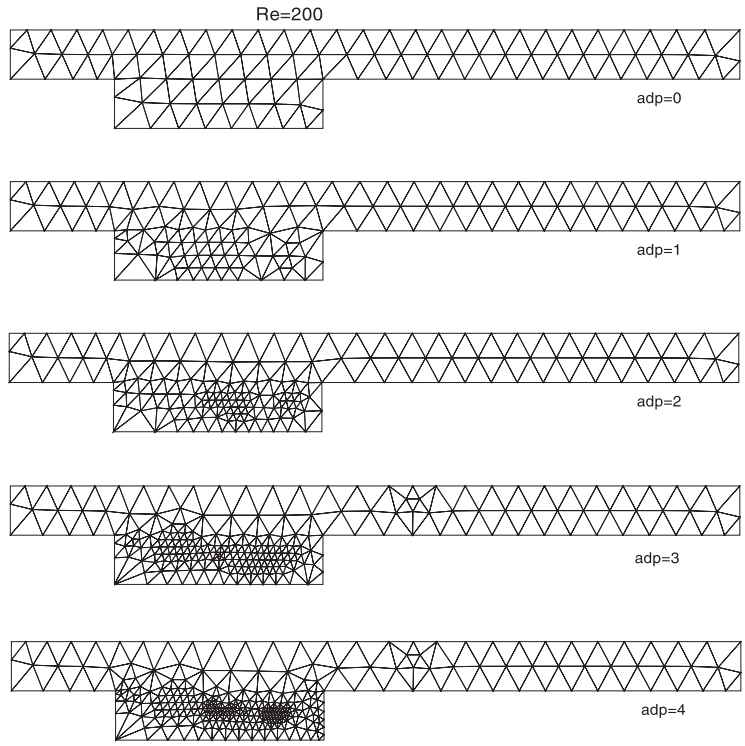

Figure 4.
Adaptive refinement of a coarse grid for flow over a cavity, using the velocity angle error estimator, $e_\theta = \sum \int_{\Omega^e} [(\hat{\theta}_x - \bar{\theta}_x)^2 + (\hat{\theta}_y - \bar{\theta}_y)^2] d\Omega^e$, $Re = 200$.

refined by using the Zienkiewicz and Zhu error estimator e_{ZZ} are presented in Figure 5. It is known that the Zienkiewicz and Zhu error estimator (Zienkiewicz and Zhu, 1987) is sensitive to high strain areas, and thus, as shown in Figure 5, adaptive regions as refined using the *ZZ* estimator are concentrated around the top two corners of the cavity. Numerical simulation in other *Re* cases (*Re* from 10 to 800) confirms that the *ZZ* estimator fails to detect wakes and reattachment regions, and more nodes added to the top two corners does not help to capture the details of those circulation zones. By using e_θ as an error indicator, those cells which have significant change of velocity direction with respect to their neighboring cells are refined. It is known from the simulation that this adaptive indicator e_θ focuses more refined nodes on circulation zones and the error is dilutely distributed on the whole computational domain.

The finite element computation is conducted on the adaptive grids, and Figure 6 presents streamlines drawn from the velocity approximation for the Reynolds number ranging from 10 to 800. The center of the recirculation zone moves towards the left as *Re* increases, and since refined grids follow well with the large eddy, the indicator e_θ is seen to provide a good grid resolution to resolve flow features. It is noted that as the adaptive scheme goes to deep

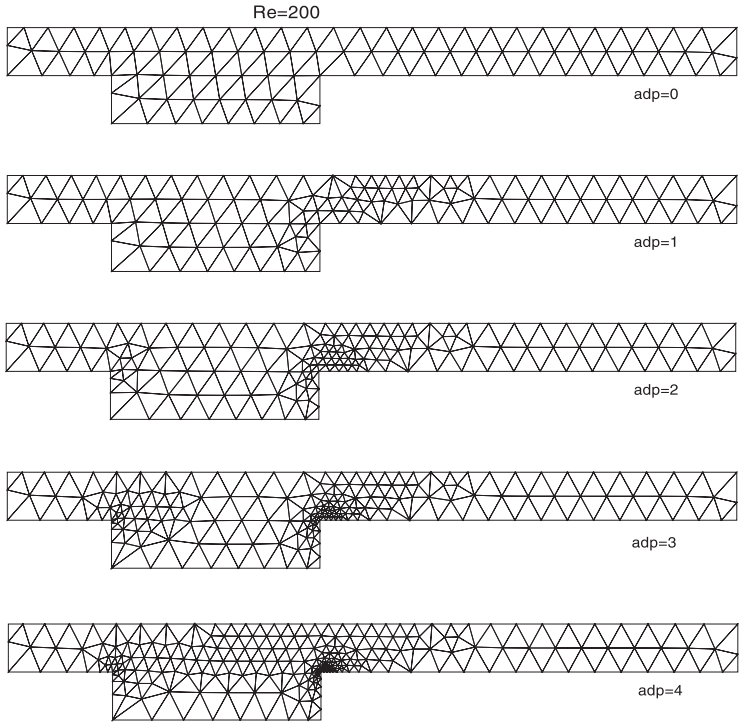

Figure 5.
Adaptive refinement of a coarse grid for flow over a cavity, using the Zienkiewicz and Zhu error estimator, $e_{ZZ} = \sum \int_{\Omega^e} [(\hat{\varepsilon}_{xx} - \bar{\varepsilon}_{xx})^2 + (\hat{\varepsilon}_{yy} - \bar{\varepsilon}_{yy})^2 + 2(\hat{\varepsilon}_{xy} - \bar{\varepsilon}_{xy})^2] d\Omega^e$, $Re = 200$.

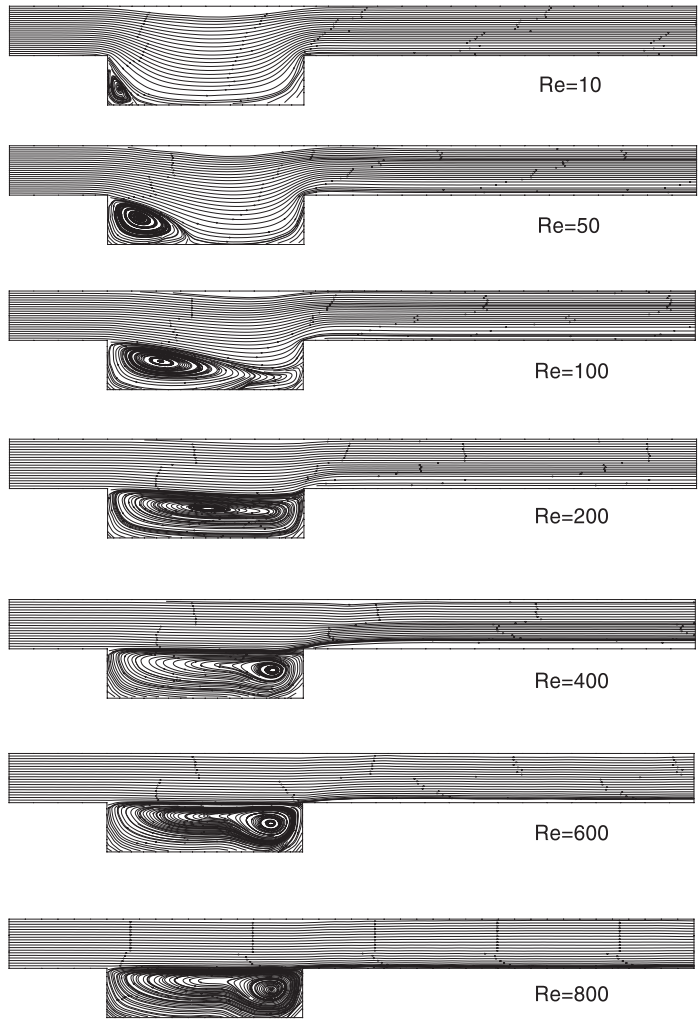

Figure 6.
Streamlines for flow over a cavity. *Re* is ranged from 10 to 800, the flow field is solved using the adaptive grid

levels, the refinement grid resolves small eddies at the two bottom corners of the cavity. The strength of the eddies are very weak and the details of each bubble (e.g. $Re = 600$) are shown in Figure 7. As known from the numerical simulations, when $Re > 400$, the center of the large eddy does not move significantly. However, the small eddy which is located at the left bottom corner becomes relatively larger as *Re* increases. These counter-rotating eddies which are embedded within the primary circulation zone are consistently predicted in all simulations.

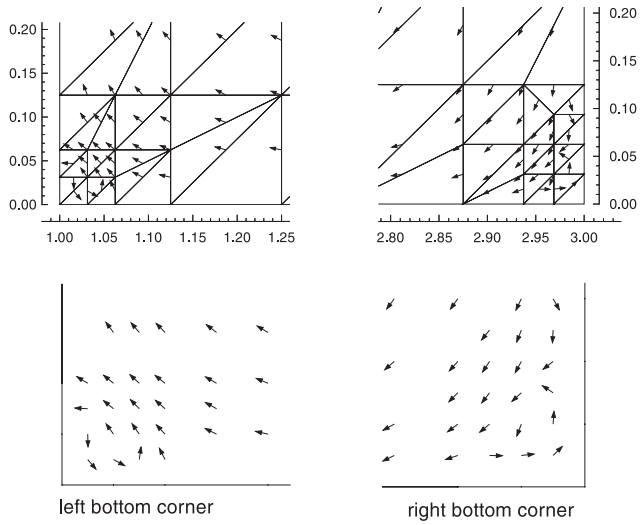

Figure 7.
The counter-rotating eddies which are located at the left and right corners of the cavity are detected; the velocity vector represent flow direction only, $Re = 600$.

4.2 Flow in a ∏-shaped pipe

Flow in a ∏-shaped pipe is also investigated through the adaptive approach. The initial inlet velocity is specified by a parabolic profile with the average velocity set to unity and Neumann boundary conditions are imposed at the exit. A configuration of this flow case is illustrated in Figure 8.

The adaptive grid results and the corresponding streamlines for the flow in a ∏-shaped pipe are shown in Figure 9. It is seen that the three vortices, one large vortex located at the side wall and two corner vortices located at the top wall, are resolved clearly using the velocity angle error estimator e_θ. The details of the three vortices are shown in Figure 10 and the flow is solved at the adaptive level 6 (the total unknowns are $Nt = 2224$, for adp = 6). Note that the

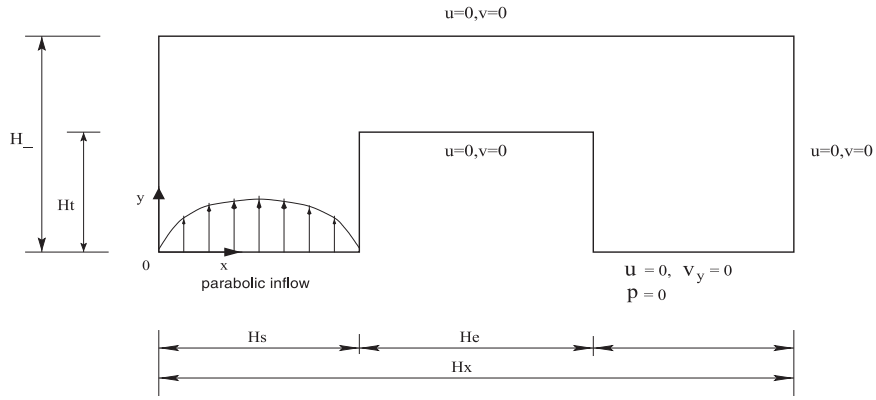

Figure 8.
Schematic of flow in a ∏-shaped pipe

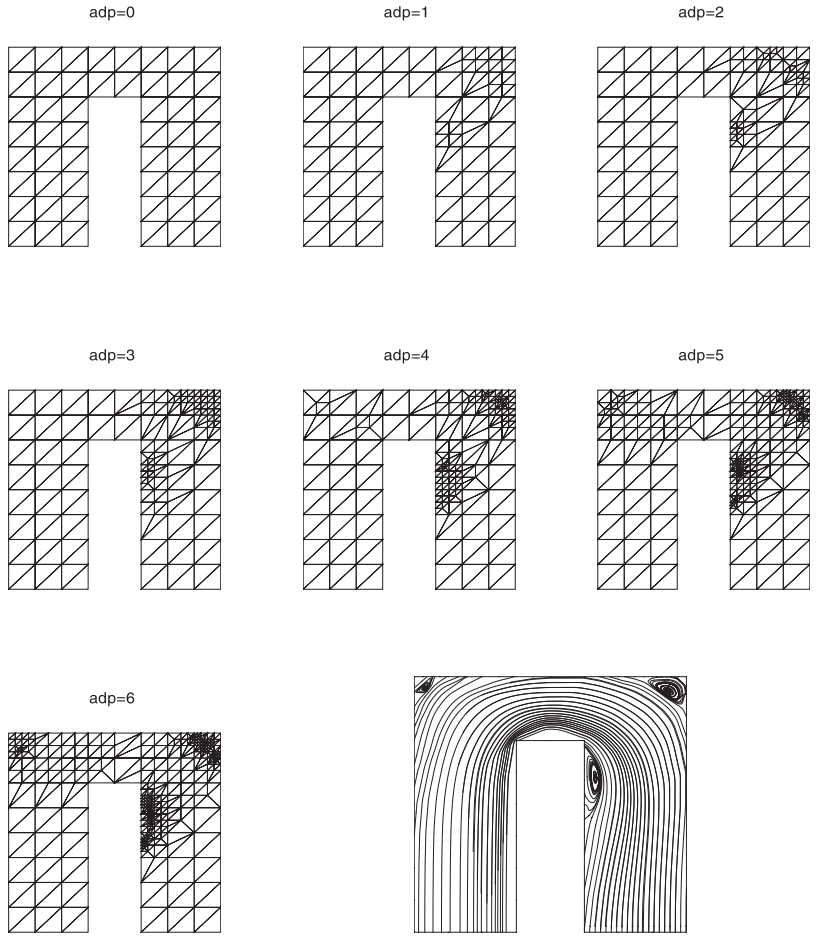

Figure 9.
Adaptive refinement of a coarse grid for flow in a $\prod$-shaped pipe, using the velocity angle error estimator, $e_\theta = \sum \int_{\Omega^e} [(\hat{\theta}_x - \bar{\theta}_x)^2 + (\hat{\theta}_y - \bar{\theta}_y)^2] d\Omega^e$, $Re = 100$.

location of the separation points and the reattachment points are resolved precisely as Figure 10 indicates. Figure 11 shows the finite element simulation using the Zienkiewicz and Zhu error estimator (Zienkiewicz and Zhu, 1987) and the adaptive results show that the refinement regions are concentrated around the two corners of the interior wall.

To be able to detect flow features efficiently and to resolve them precisely are the requirements of solving viscous incompressible flows. It is seen that the e_θ estimator can identify separation points and reattachment points accurately and use less unknowns. The tests show that, if other estimators are used, at least 20 times more equations (or unknowns) are needed to reach the same precise location of these flow features.

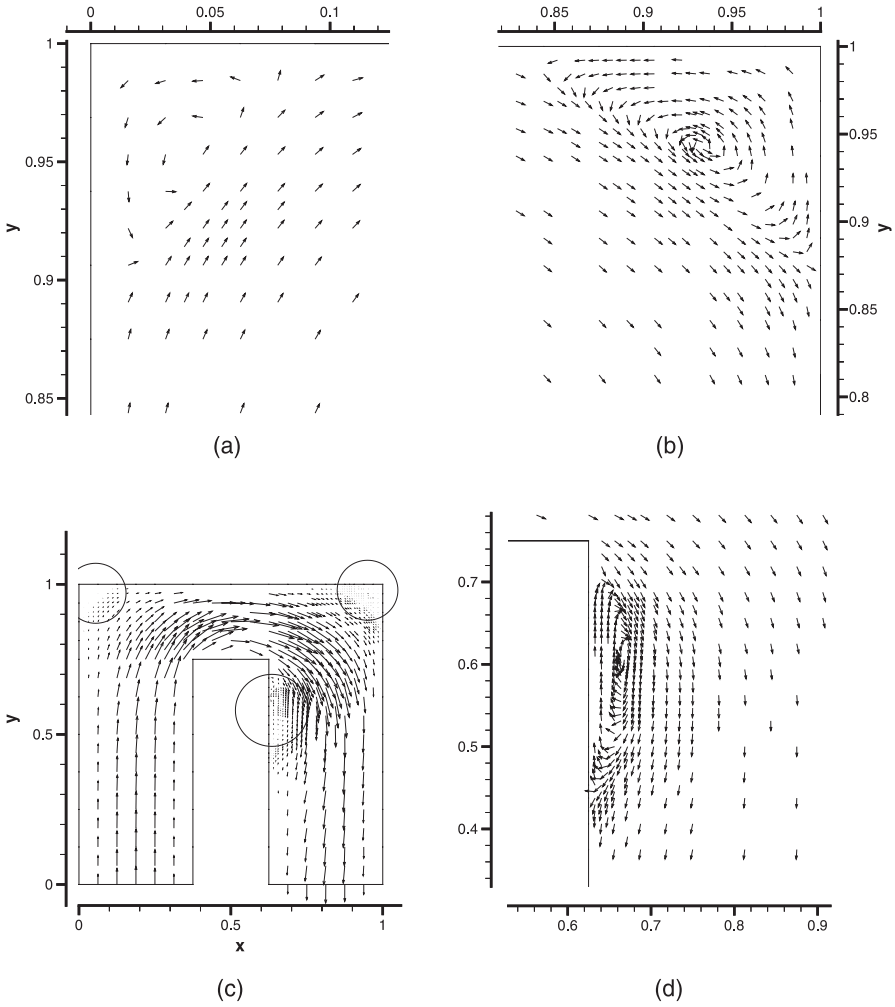

Figure 10.
Three vortices are resolved using the velocity angle error estimator e_θ. (a): The vortex located at the left top corner. (b): The vortex located at the right top corner. (c): The flow field. (d): The vortex located at the interior side wall. In (a)(b)(d), the velocity vector has a uniform length, showing flow direction. In (c), the velocity vector is proportional to velocity amplitude. $Re = 100$.

4.3 Flow in a sludge tank

The simulation of flow in a sludge tank is a practical case which has an application in the car painting industry. In this flow, to detect vortices efficiently, and more specifically, to resolve the location of the eddies precisely, is a key concern to an efficient utilization and maintenance of the sludge tank. A geometric description of this flow case is illustrated in Figure 12. The nozzle which is located at the top of the wall is the inlet flow, and it tilts 45-degrees towards the left wall.

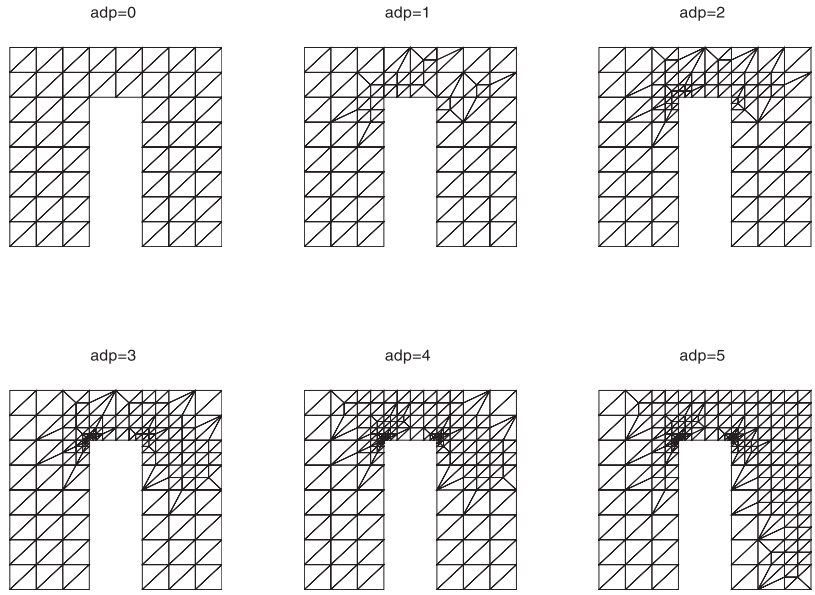

Figure 11.
Adaptive refinement of a coarse grid using the Zienkiewicz and Zhu error estimator, $e_e = \sum \int_{\Omega^e} [(\hat{\varepsilon}_{xx} - \bar{\varepsilon}_{xx})^2 + (\hat{\varepsilon}_{yy}\Omega\bar{\varepsilon}_{yy})^2 + 2(\hat{\varepsilon}_{xy}\Omega\bar{\varepsilon}_{xy})^2] d\Omega^e$, $Re = 100$.

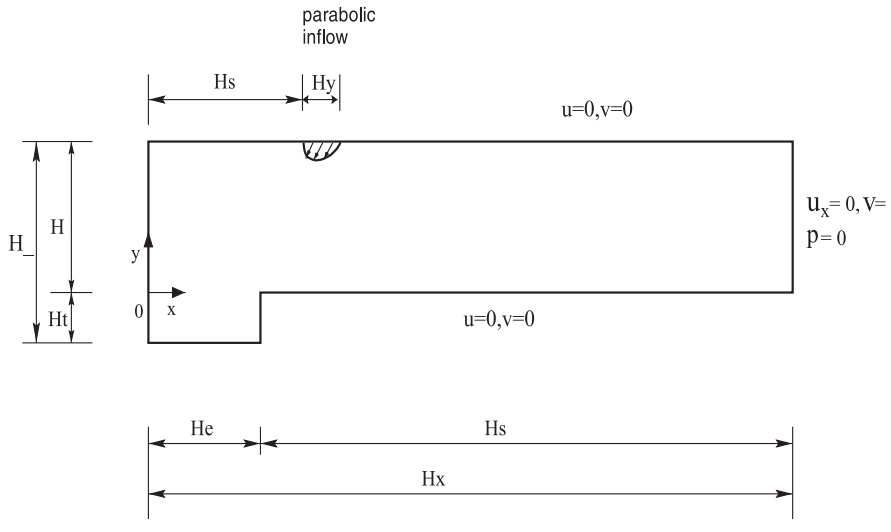

Figure 12.
Schematic of flow in a sludge tank

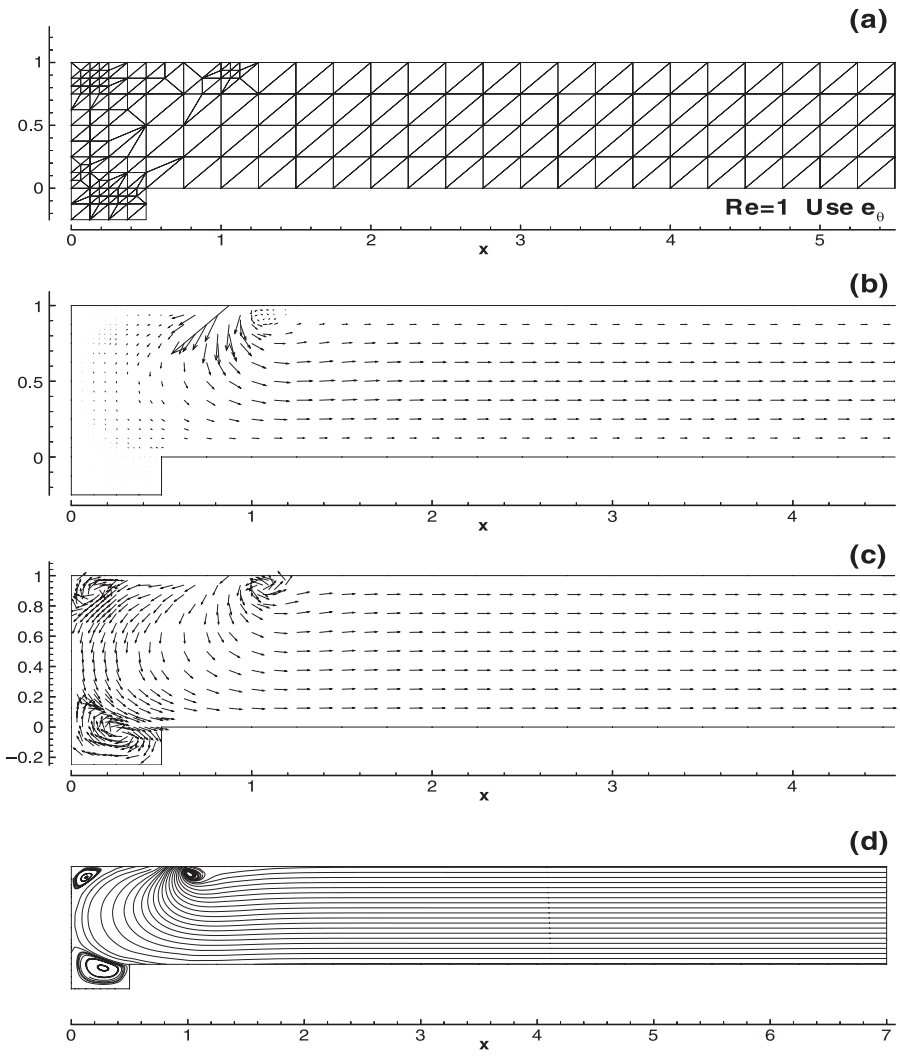

Figure 13.
Flow in a sludge tank, using e_θ, $Re = 1$. (a): adaptive mesh, (b): velocity vector in the computational domain, the length of velocity vector is proportional to velocity amplitude, (c): the velocity vector has a uniform length, showing flow direction only, (d): the streamlines of the above vector fields

For the $Re = 1$ case and the $Re = 10$ case, three vortices, one located at the left bottom of the tank, one located in the left top corner, and one located at the right side of the nozzle, are resolved clearly by using the e_θ estimator (Figure 13). For the $Re = 50$ case, the three vortices become larger when the Reynolds number increases (in comparison with the $Re = 10$ case), and the left bottom vortex and the left top vortex begin to touch each other.

For the $Re = 100$ case, the velocity profiles and streamlines are shown in Figure 14. As Figure 14 indicates, the vortex located at the right side of the nozzle continues to grow larger when the Reynolds number increases. When Re

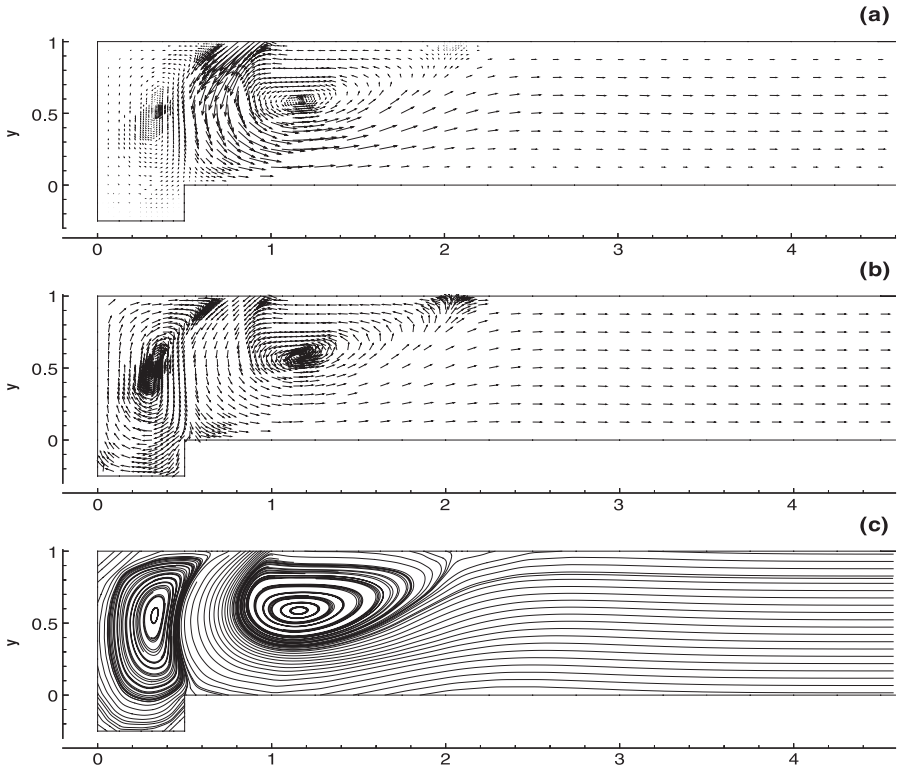

Figure 14.
Flow in a sludge tank, $Re = 100$. (a): velocity vector in the computational domain, the length of velocity vector is proportional to velocity amplitude, (b): the velocity vector has a uniform length, showing flow direction only, (c) the streamlines of the above vector fields

reaches 100, the left bottom eddy and the left top eddy join each other to become one primary vortex. As seen from Figure 14(b), there are counter-rotating eddies embedded within the left primary circulation zones (located at the bottom of the tank), and the strength of the eddies is very weak. These small eddies get weaker as Re decreases, but, through using e_θ, they are still visible in the bottom wall corners at deeper levels of adaptive grids.

For the $Re = 200$ case, an additional primary vortex located near the bottom wall is found. For the $Re = 300$ case (Figure 15) and the $Re = 400$ case, the vortex located at the right bottom wall becomes larger as Re increases, and the separation point and the reattachment point move towards the right as well. There are counter-rotating eddies embedded within the left primary circulation zone and they are located in the bottom corners of the sludge tank. These eddies are resolved precisely using the e_θ estimator.

The adaptive mesh results obtained by using the velocity angle estimator are summarized in Figure 16 (for Reynolds numbers from 1 to 400). For the same Re range, Figure 17 presents the corresponding streamlines drawn from the computed velocity field. It is seen that the eddies in the sludge tank are

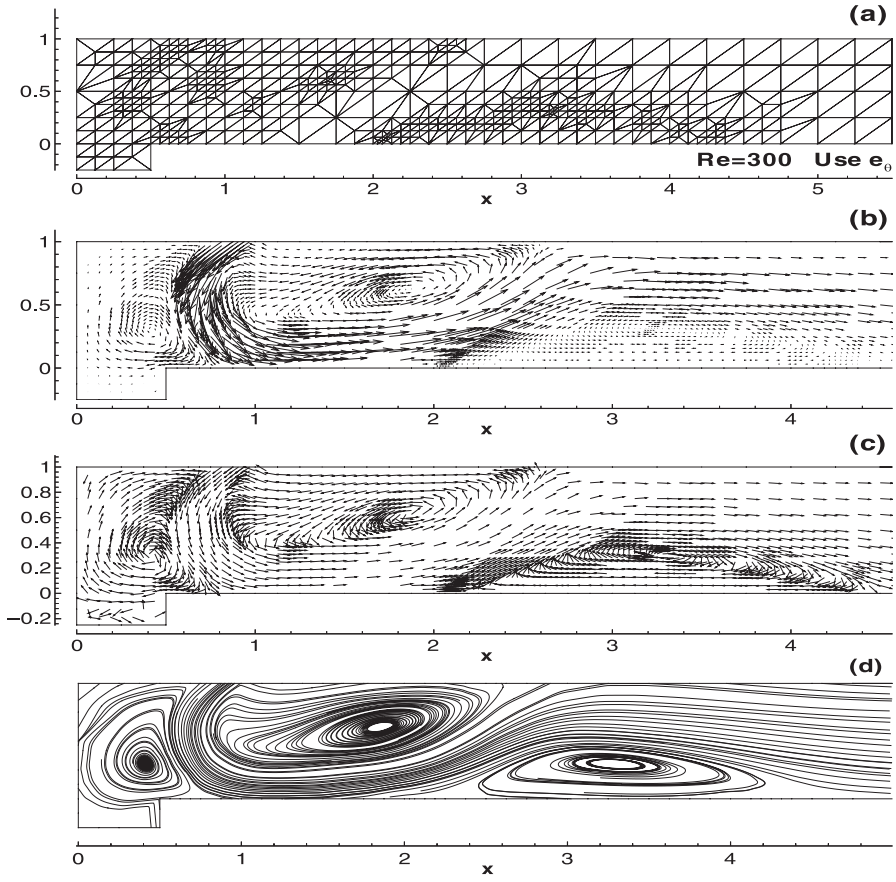

Figure 15.
Flow in a sludge tank, using e_θ, $Re = 300$. (a): adaptive mesh, (b): velocity vector in the computational domain, the length of velocity vector is proportional to velocity amplitude, (b): the velocity vector has a uniform length, showing flow direction only, (d) the streamlines of the above vector fields

clearly visible and resolved, and flow features are captured in precise details by employing the e_θ estimator. It is concluded from numerous tests that the adaptive grids using e_θ follow the vortices development and match flow features with fewer unknowns.

5. Conclusions

The conclusions reached in this paper can be summarized as follows:

First of all, the velocity angle error estimator is a curvature error estimator, and its value reflects the accuracy of the curvature k. The velocity angle error estimator is also a streamline error estimator and this is true for both steady and unsteady flows. Comparing $\hat{\theta}_s$ and $\check{\theta}_s$ or comparing $\hat{k}$ and $\check{k}$ represents the velocity angle error e_θ. As the velocity angle error is reduced by using the e_θ estimator, approximate curves are asymptotic to the true curves, or the approximate streamlines are asymptotic to the true streamlines. Thus, the e_θ

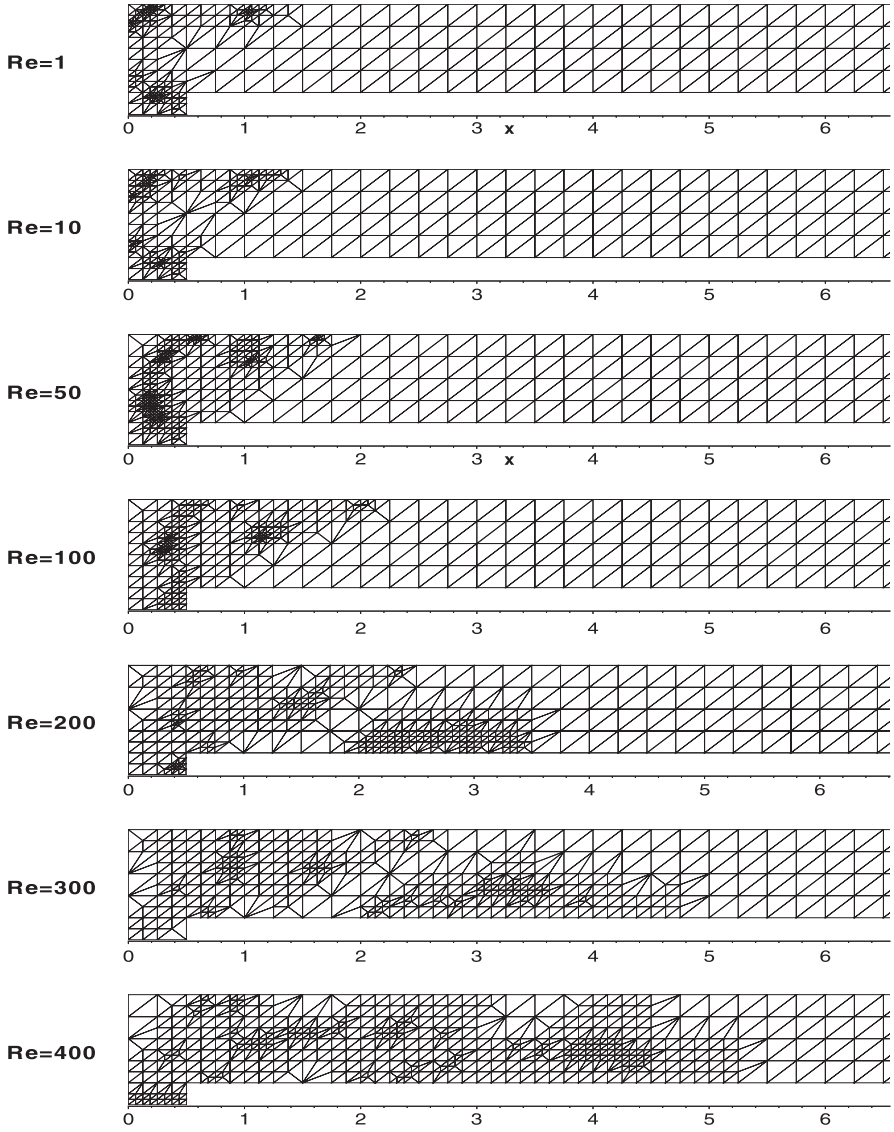

Figure 16.
Adaptive refinement of a coarse grid for flow in a sludge tank; *Re* ranges from 1 to 400, using velocity angle error indicator, $e_\theta = \sum \int_{\Omega^e} [(\hat{\theta}_x - \bar{\theta}_x)^2 + (\hat{\theta}_y - \bar{\theta}_y)^2] d\Omega^e$.

estimator can be viewed as an efficient instrument to reduce the curvature roughness, and as an adaptive indicator, to guide the mesh density to reach a precise k and precise streamlines.

Secondly, the velocity angle error estimator contains the nonlinear convective term of the Navier-Stokes equations. When $\hat{\theta}_x$ is asymptotic to $\bar{\theta}_x$, or the true θ_x, the calculated value of a_y is asymptotic to the true value of a_y. When

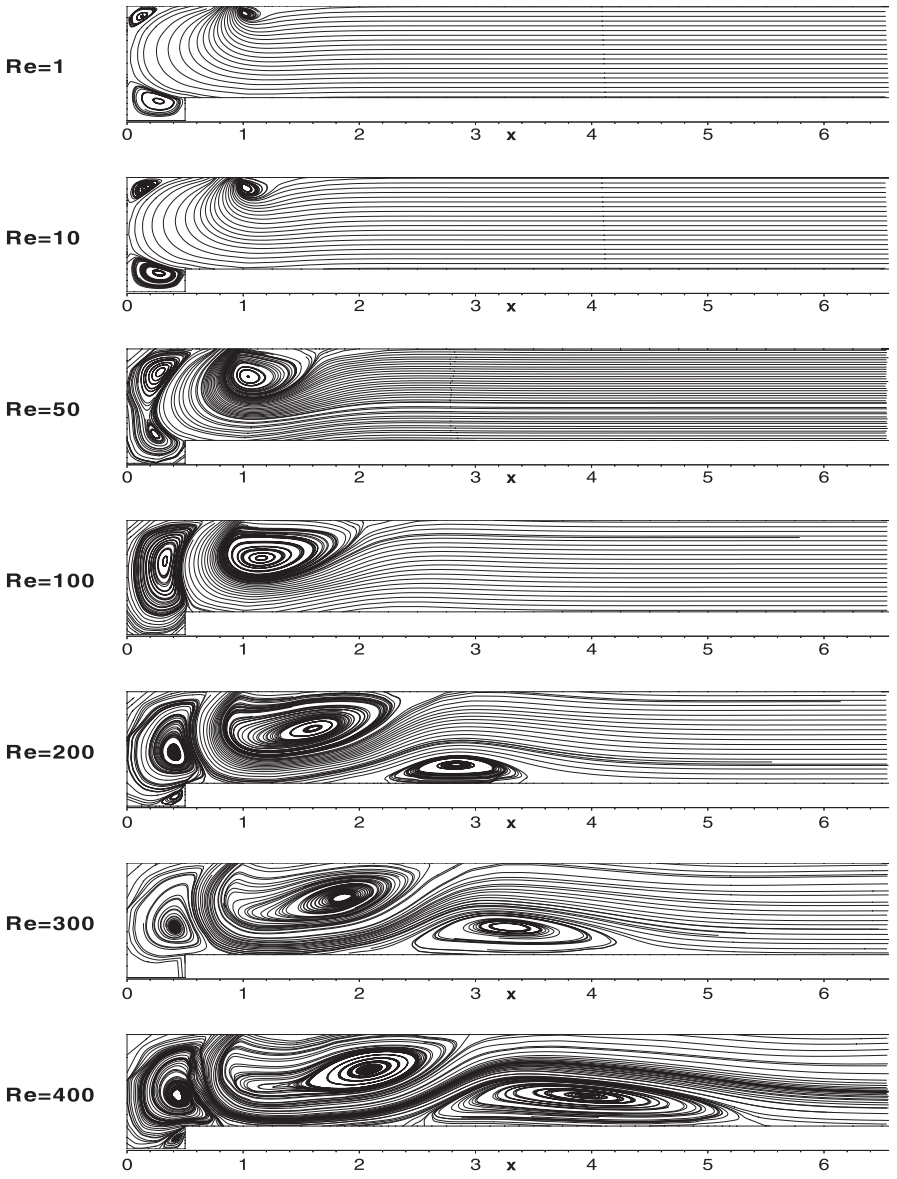

Figure 17.
Streamlines for flow in a sludge tank; *Re* ranges from 1 to 400

$\hat{\theta}_y$ is asymptotic to $\bar{\theta}_y$, or the true θ_y, the calculated a_x is asymptotic to the true value of a_x. In other words, as the velocity angle error is reduced by using the e_θ estimator, the error on the convective acceleration decreases, and a_x and a_y become more accurate.

Thirdly, the velocity angle error estimator represents the difference between the acceleration direction and the velocity direction. The e_θ estimator can be expressed as ($\tan\Phi - \tan\theta$) convective acceleration/Λ^2). When the convective acceleration direction, Φ, and the flow velocity direction, θ, become disparate, the curvature k is not zero, and flow changes occur. More importantly, e_θ identifies those regions where two directions have a discrepancy and it computes the error accordingly. The larger the difference between $\tan\Phi$ and $\tan\theta$, the greater is the curvature k. Moreover, the larger the variations of the direction difference, the larger is the value of the e_θ error, and thus the denser the grids where two directions have a disparity.

The numerical tests verify that the velocity angle error estimator e_θ can detect most flow characteristics and produce dense grids in the appropriate regions (e.g. the regions where flow velocity directions have abrupt changes). The refinement grids using e_θ follow changes of eddies and reattachment points when the Reynolds number varies. The e_{ZZ} fails to detect vortices and concentrates grids in high strain regions (e.g. the internal corners of the $\prod$-shaped pipe). The adaptive results justify the applicability of the e_θ estimator and prove that this error estimator is a valuable adaptive indicator for the automatic refinement of unstructured grids.

References

Axelsson, O. and Barker, V.A. (1984), *Finite Element Solution of Boundary Value Problems, Theory and Computation*, Academic Press, Inc., Orlando.

Baker, T.J. (1997), "Mesh adaptation strategies for problems in fluid dynamics", *Finite Elements in Analysis and Design*, 25, pp. 243-73.

Babuška, I., Strouboulis, T. and Upadhyay, C.S. (1994), "A model study of the quality of à-posteriori error estimators for linear elliptic problems", *Comp. Meths. in Appl. Mech. and Eng.*, 114, pp. 307-78.

Babuška, I., et al., (1994), "Validation of à-posteriori error estimators by numerical approach", *Int. J. for Numerical Methods in Engineering*, 37, pp. 1073-123.

Cuvelier, C., Segal, A. and van Steenhoven, A.A. (1986), *Finite Element Methods and Navier-Stokes Equations*, D. Reidel Publishing Company, Dordrecht.

Ewing, R.E. (1990), "A posteriori error estimation", *Comp. Meths. in Appl. Mech. and Eng.*, 82, pp. 59-72.

Fuenmayor, F.J., Oliver, J.L. and Rodenas, J.J. (1997), "Extension of the Zienkiewicz-Zhu error estimator to shape sensitivity analysis", *Intl. J. for Numerical Methods in Engineering*, 40, pp. 1413-33.

Girault, V. and Raviart, P. (1986), *Finite Element Methods for Navier-Stokes Equations, Theory and Algorithms*, Springer-Verlag, Heidelberg.

Habashi, W.G., et al., (1994), "Large-scale computational fluid dynamics by the finite element method", *Intl. J. for Numerical Methods in Fluids*, 18, pp. 1083-105.

Lee, D. and Tsuei, Y.M. (1992), "Modified adaptive grid method for recirculation flows", *Intl. J. for Numerical Methods in Fluids*, 14 No. 7, pp. 775-91.

Oden, J.T., Wu, W.H. and Legat, V. (1995), "An hp adaptive strategy for finite element approximations of the Navier-Stokes equations", *Intl. J. for Numerical Methods in Fluids*, 20, pp. 831-51.

Pironneau, O. (1989), *Finite Element Methods for Fluids*, Masson, Paris.

Wu, H. An à-posteriori finite element error estimator for adaptive grid computation of viscous incompressible flows PhD Thesis Univ. of Toronto, Toronto.

Wu, H. and Currie, I.G. (1997), *Numerical simulation of viscous incompressible flows using posteriori error estimation*, Proceedings of CFD 97, Univ. of Victoria, Victoria, BC pp. 525-30.

Wu, H. and Currie, I.G. (2000), "An adaptive mesh refinement using à-posteriori finite element error estimation", *Transactions of the CSME*, 24, pp. 247-61.

Zhu, J.Z. (1997), "À-posteriori error estimation - the relationship between different procedures", *Comp. Meths. in Appl. Mech. and Eng.*, 150, pp. 411-22.

Zienkiewicz, O.C. and Zhu, J.Z. (1987), "A simple error estimator and adaptive procedure for practical engineering analysis", *Intl. J. for Numerical Methods in Engineering*, 24, pp. 337-57.